

HEDRA: A Bio-Inspired Modular Tensegrity Robot With Polyhedral Parallel Modules

Vishal Ramadoss*, Keerthi Sagar*, Mohamed Sadiq Ikbai, Jesus Hiram Lugo Calles,
Raghubeer Siddaraboina and Matteo Zoppi

Abstract— There is a surge of research interest in the field of tensegrity robotics. Robots developed under this paradigm provide many advantages and have distinguishing features in terms of structural compliance, dexterity, safety, and weight reduction. This paper proposes a new robotic mechanism based on tensegrity ('tension-integrity') robots and reconfigurable modular robots. The specific actuation schemes for this tensegrity robot with multiple degrees of freedom are presented. This article describes an easy-to-assemble 350 mm tensegrity-based robot prototype by stacking a series of rigid polyhedrons linked with tensegrity joints that have no direct rigid contact with each other. The functionality of the proposed robot is validated by the experimental results by integrating the polyhedral parallel structure as its skeleton and series of tensegrity joints. The reachable workspace of the proposed manipulator was determined and the range of motion analysis was performed. The pilot evaluation demonstrated three working phases including axial twist, compression and bending motion of the presented design. The large bending angle and deployability shown in the tests proved the functionality of the lightweight tensegrity robot.

I. INTRODUCTION

Traditional rigid robots are fast and precise systems that are used in manufacturing environments. The advent of collaborative robots have significantly reduced the costs and have the ability to work safely alongside humans. This has led to the evolution towards human friendly robotics. In parallel, soft robotics have garnered widespread attention and offers solutions that cannot be addressed by robots built from rigid bodies. An alternative design methodology to either rigid or soft robots are tension-integrity systems.

The emerging field of tensegrity robotics aims to combine the advantages of conventionally stiff and the continuous compliant mechanisms. This results in a smaller form factor with regards to the footprint of the robot and lower power requirements. Novel applications are being proposed for robotic systems such as robots for space explorations [1], search and rescue and rehabilitation. Such robots are pioneering soft robotic concepts [2] which combine biomimetics and tensegrity frameworks. They are lightweight, reconfigurable [3] and compliant [4] similar to soft robots and performs complex motions. Tensegrity demonstrates the natural bal-

ance of forces where the compression members are suspended in the dynamic tension network.

Significant work has been done to leverage the concepts of tensegrity in robotic systems, which transforms their shape thereby performing crawl [5], swim [6] [7], roll, climb [8] and fly [9]. The contribution in the field of biotensegrity [10][11] produced manipulators that emulate the human elbow [12], arm [13], shoulder [14] and vertebrae [15] [16]. The open loop stable manipulation control of a soft manipulator was studied in [17] and a control strategy based on array of sensors was investigated in [18].

Existing frameworks results in configuration with a large number of bars and cables making fabrication and assembly challenging with constraints on space for actuators and sensors. Owing to this fact, most of the 'bar-only' tensegrities are tested in simulation or workbenches. There is a need for an archetype to bridge the gap between simulation and hardware, that allows innovative bio-inspired geometries rather than limiting the forms of tensegrity. Bioinspired vertebrae morphologies are utilized and its geometric compliance is exploited to simplify the design process. This is the motivation behind the development of our proposed bio-inspired modular tensegrity soft robot with polyhedral parallel modules (HEDRA) as shown in Figure 1.

The contributions of this work can be summarized as:

- A low-cost, lightweight, easy to assemble modular robot

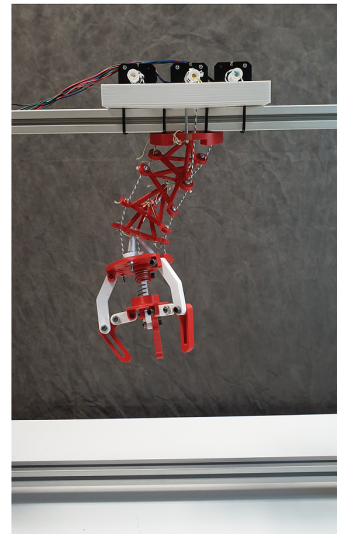


Fig. 1: Hedra at stowed configuration

* Equal contribution. V. Ramadoss, K. Sagar, M.S. Ikbai, J.H. Lugo Calles, R. Siddaraboina and M. Zoppi are with PMAR Robotics Group, Department of Mechanical, Energy, Management and Transportation Engineering, University of Genoa, Genoa (GE), 16145, Italy. Email: {keerthi, lugocalles, zoppi}@dimec.unige.it, {vishal.ramadoss, mohamedsadiq.ikbai, S5089493@studenti.unige.it}@edu.unige.it

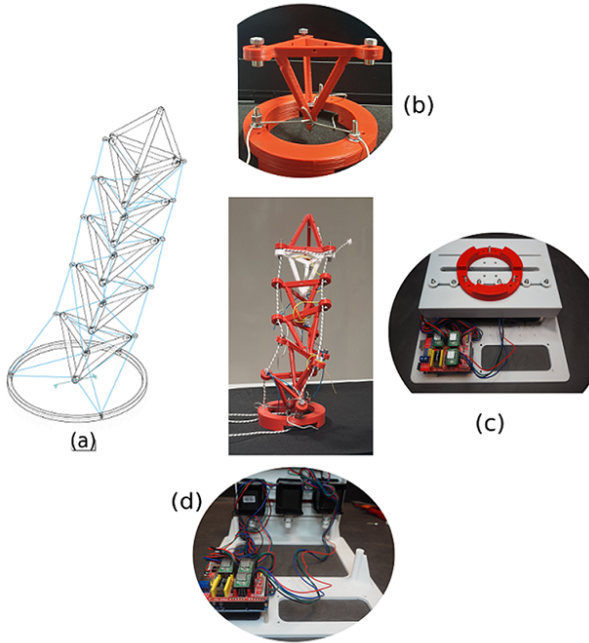


Fig. 2: (a) Wireframe of tensegrity manipulator with tetrahedral parallel modules with 3-Dof tensegrity joints (b) The structure of tensegrity joint with axial and horizontal tension network. The cable outlets are fixed by the bolts and nuts. (c) base plate with barrel jack connectors equipped with motor drivers powering the tensegrity module (d) closer view of the interface between motors and motor driver

which have distinct softness with granular rigidity for education and research;

- An alternative to conventional rigid robotic mechanisms with advantages of compliance and variable stiffness of redundant serial-parallel robots;
- Minimal design changes while stacking modules and addition of parallel stages with ability to build into closed-loop and tree robots;

In what follows, we first describe the concept design and fabrication, including the overall geometry of the proposed robot in Section II. A simple modeling framework is described in Section III. The simulations and proof-of-concept is elucidated in Section IV. The concluding remarks are drawn in Section V.

II. MATERIALS AND METHODS

A. Concept design and Fabrication

Fig. 1 shows the overall structure of the bio-tensegrity robot in stowed configuration. It is composed of five tetrahedral rigid platforms which are linked with vertical tensile cables and one tetrahedron at the top serving as end-effector equipped with tool mount. Structural compliance is achieved due to the elastic property of tensile components.

The tetrahedron acts as the compression element of the tensegrity joint. The tensile elements are the cables that are divided into two groups, the horizontal saddle cables

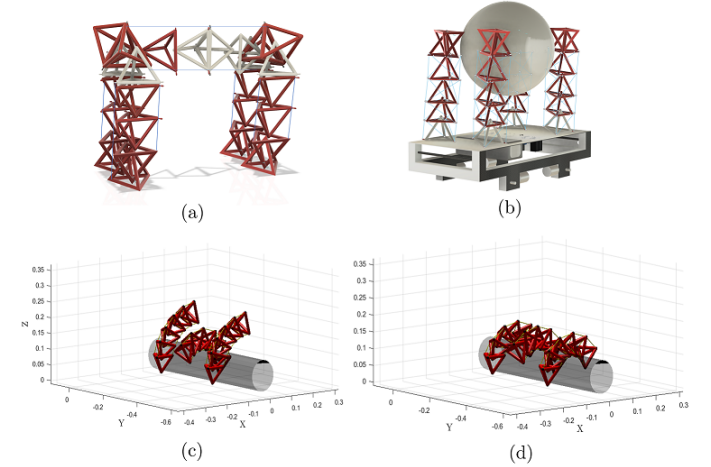


Fig. 3: a) Rendering of tensegrity quadruped with compliant tensegrity spine b) Rendering of tensegrity structure based quadruped in inverted configuration as gripper c) Inverse kinematic simulation of three fingered soft robotic gripper d) Grasping of cylindrical objects

and the axial cables as shown in Fig. 4. The cable tension forces acting axially serve to pull the stacked tetrahedra together. The horizontal tension network is connected from the bottom node of the top tetrahedra to support the bottom tetrahedra in suspension. The top tetrahedra is under downward tension due to the axial tension network and also the saddle cables can serve the upward tension and resist the downward forces. This resistance from the saddle cables is augmented to the overall network of tensegrity joints and the load is distributed. This is the primary reason behind the motion of the top tetrahedron around the bottom tetrahedron without direct contact thereby acting as tensegrity joint. Then, the tensegrity joints are connected in series to have a stacked manipulator. The joint has 3 degrees of freedom having a virtual ball joint center at the center of saddle cable network as shown in Fig. 2(b). In order to transform the redundant series-parallel mechanisms into a compliant mechanism, bioinspired backbone and lamprey morphologies are utilized.

The robot core entity, the tetrahedron and the base are 3D printed in PLA, diameter 1.75 mm, using Delta Wasp 3D printer. An octahedron topology is chosen as end-effector for mounting the Intel Realsense D435i camera (260 gms). A three finger linkage based gripper mechanism weighing 280 gms is developed separately to perform grasping. The prototype is driven by three active cables made of Dyneema ultra-high molecular weight polyethylene (UHMWP) wires with diameter of 2mm and Young's Modulus of 110 GPa. The saddle cables are taut using Spectra Extreme Braid fishing line with diameter of 0.68 mm and with load capacity of 60 kgs. NEMA 17 stepper motors with A4988 motor drivers were used for the pilot evaluation of the manipulator in the laboratory setup to visualize the bending and axial twist motion.

Different cable routing schemes have been proposed pre-

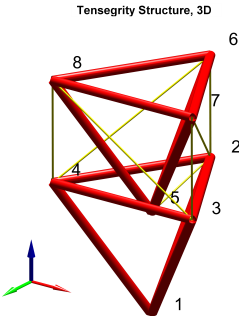


Fig. 4: A three-dimensional, tetrahedral tensegrity manipulator. Black dots are nodes, red edges are bars (compressive), and yellow edges are cables (tension). x-,y-,z- axis is denoted by red, green and blue color respectively.

viously for multi link cable driven robots. We initially model with minimally actuated cable setup with 3 active cables and investigate the clustered actuation model with 6 active cables based on the previous works on actuation strategy. For experiments, minimally actuated HEDRA is utilized. The design parameters of the unit tetrahedron is given in the Table. I.

TABLE I: Design parameters of the unit tetrahedron

Parameter	Value
Edge length	70 mm
Height from the base	51.48 mm
Edge thickness	3 mm
Weight	14 g

III. TOPOLOGICAL NOTATION

A tensegrity structure is defined by a graph $G = (V, E)$, with nodes V and edges E . There are n nodes, where each $\mathbf{a}_i \in V$, $i = 1 \dots n$ represents a point in \mathbb{E}^3 where the structural members connect. There are m edges, where each edge $e_k \in E$, $k = 1 \dots m$ represents a structural member that connects two nodes. Forces $P = \{\mathbf{p}_1, \dots, \mathbf{p}_n\}$, $\mathbf{p}_i \in \mathbb{E}^3$ are applied at each node. Let $\mathbf{x}, \mathbf{y}, \mathbf{z} (\in \mathbb{R}^n)$ denote the nodal coordinate vectors in the x, y and z directions. The structural members consists of r bars that can take compression or tension loading, or s cables, that can only take tension loading. The connectivity information of members can be expressed by the branch-node or incidence matrix, $\mathbf{C} \in (\mathbb{R}^{(s+r) \times n})$. If member $i \in \{1, \dots, (s+r)\}$ connects nodes k and j ($k < j$), then the k -th and j -th columns in \mathbf{C} are set to 1 and -1 respectively, as

$$\mathbf{C}^{(u,v)} = \begin{cases} 1 & \text{if } u = i, v = k \\ -1 & \text{if } u = i, v = j \\ 0 & \text{if else} \end{cases} \quad (1)$$

For the tensegrity structure shown in Fig. 4, the connec-

tivity matrix is given by

$$\mathbf{C}_s = \left[\begin{array}{cccccc|cccc} 0 & 1 & 0 & 0 & -1 & 0 & 0 & 0 \\ 0 & 0 & 1 & 0 & -1 & 0 & 0 & 0 \\ 0 & 0 & 0 & 1 & -1 & 0 & 0 & 0 \\ 0 & 1 & 0 & 0 & 0 & -1 & 0 & 0 \\ 0 & 1 & 0 & 0 & 0 & 0 & -1 & 0 \\ 0 & 0 & 1 & 0 & 0 & 0 & -1 & 0 \\ 0 & 0 & 1 & 0 & 0 & 0 & 0 & -1 \\ 0 & 0 & 0 & 1 & 0 & 0 & 0 & -1 \\ 0 & 0 & 0 & 1 & 0 & -1 & 0 & 0 \end{array} \right]$$

$$\mathbf{C}_r = \left[\begin{array}{cccccc|cccc} 1 & -1 & 0 & 0 & 0 & 0 & 0 & 0 \\ 1 & 0 & -1 & 0 & 0 & 0 & 0 & 0 \\ 1 & 0 & 0 & -1 & 0 & 0 & 0 & 0 \\ 0 & 1 & -1 & 0 & 0 & 0 & 0 & 0 \\ 0 & 1 & 0 & -1 & 0 & 0 & 0 & 0 \\ 0 & 0 & 1 & -1 & 0 & 0 & 0 & 0 \\ 0 & 0 & 0 & 0 & 1 & -1 & 0 & 0 \\ 0 & 0 & 0 & 0 & 1 & 0 & -1 & 0 \\ 0 & 0 & 0 & 0 & 1 & 0 & 0 & -1 \\ 0 & 0 & 0 & 0 & 0 & 1 & -1 & 0 \\ 0 & 0 & 0 & 0 & 0 & 1 & 0 & -1 \\ 0 & 0 & 0 & 0 & 0 & 0 & 1 & -1 \end{array} \right]$$

$$\mathbf{C} = \begin{bmatrix} \mathbf{C}_s \\ \mathbf{C}_r \end{bmatrix} \quad (2)$$

where \mathbf{C}_s (indicated in blue) represents the cable connectivity with $s = 9$ cables and \mathbf{C}_r (indicated in red) represents the bar connectivity with $r = 12$ bars and the size of \mathbf{C} for the robot in Fig. 4 is 21×8 . The lighter color represent the nodes for the bottom tetrahedron which is fixed to the ground and the dark-shaded rows represent the moving tetrahedra.

The biotensegrity robot, in general has n tetrahedrons, in three dimensions. The radius of the tetrahedron is r and the origin of the coordinate system is at the common point of the lowermost tetrahedron, where the flat polygon base and the triangular faces are connected. The initial coordinates of the base tetrahedron are parameterized as

$$\mathbf{S}_i = \begin{bmatrix} r \sin(0) & r \cos(0) & h \\ r \sin(\alpha) & r \cos(\alpha) & h \\ r \sin(-\alpha) & r \cos(-\alpha) & h \end{bmatrix} \quad (3)$$

where the rows are the Cartesian coordinates of each tetrahedron in space, r is radius of a circle that is inscribed by the top triangle of the tetrahedra, h is the height of the tetrahedra and $\alpha = 2\pi/3$. The state space matrix of each tetrahedron is defined by the three position variables due to translation and three orientation variables. After transformation of the tetrahedron, the location of points in space is represented by

$$\mathbf{S}'_i = \mathbf{S}_i R_{\theta_i, \gamma_i, \phi_i} + U T_{x_i, y_i, z_i} \quad (4)$$

where R is the rotation matrix for each Euler angle, U is the unitary matrix and T is translation matrix.

IV. CONTROL AND SIMULATION

A. Force Density Method For Inverse Kinematic Control Policy

The force density method (FDM) for solving cable network problems was described in [19]. The method used was presented in works on related topologies of tensegrity robot [8] [15]. For the sake of clarity, the static equilibrium conditions for the structure is briefly summarized. The equilibrium equations of forces at each node of the cable network is utilized to solve the inverse kinematics of the proposed tensegrity robot, with the imposed assumptions being:

- The nodes are fixed in space (known coordinates) and do not translate.
- All forces are known and are only exerted at nodes.
- The connections between the members are friction-less ball joints.
- The structural members are perfectly rigid, do not deform and do not change length.

The force balance condition in three dimensions for static equilibrium of the structure can be stated as

$$\begin{aligned} \mathbf{C}^T \text{diag}(\mathbf{q}) \mathbf{C} \mathbf{x} &= \mathbf{p}_x \\ \mathbf{C}^T \text{diag}(\mathbf{q}) \mathbf{C} \mathbf{y} &= \mathbf{p}_y \\ \mathbf{C}^T \text{diag}(\mathbf{q}) \mathbf{C} \mathbf{z} &= \mathbf{p}_z \end{aligned} \quad (5)$$

such that $\mathbf{x}, \mathbf{y}, \mathbf{z}$ represents the nodal coordinate vectors, $\mathbf{p}_x, \mathbf{p}_y, \mathbf{p}_z$ represents the external loads applied to the nodes in the x, y and z directions, $\mathbf{q} = \{q_1, q_2, \dots, q_{s+r}\}^T$ is the force density vector, where q_i is the ratio between the force, f_i , and the length, l_i , such that

$$q_i = \frac{f_i}{l_i} \quad (6)$$

The equations are reorganized in the form

$$\mathbf{A} \mathbf{q} = \mathbf{p}, \quad (7)$$

where

$$\mathbf{A} = \begin{bmatrix} \mathbf{C}^T \text{diag}(\mathbf{C} \mathbf{x}) \\ \mathbf{C}^T \text{diag}(\mathbf{C} \mathbf{y}) \\ \mathbf{C}^T \text{diag}(\mathbf{C} \mathbf{z}) \end{bmatrix} \quad \mathbf{p} = \begin{bmatrix} \mathbf{p}_x \\ \mathbf{p}_y \\ \mathbf{p}_z \end{bmatrix} \quad (8)$$

Equation (7) can be solved for \mathbf{q} using the Moore-Penrose pseudoinverse with the general solution as

$$\mathbf{q} = \mathbf{A}^+ \mathbf{p} + (\mathbf{I} - \mathbf{A}^+ \mathbf{A}) \mathbf{w}, \quad (9)$$

where $(\cdot)^+$ denotes the pseudoinverse of a matrix, \mathbf{I} is the identity matrix, and \mathbf{w} is arbitrary vector in \mathbb{R}^{3n} . The equations can be further split between the first s rows and the last r rows to denote the elements contributing to cable force densities and bar force densities such as

$$\begin{bmatrix} \mathbf{q}_s \\ \mathbf{q}_r \end{bmatrix} = \begin{bmatrix} (\mathbf{A}^+)_s \\ (\mathbf{A}^+)_r \end{bmatrix} \mathbf{p} + \left(\begin{bmatrix} \mathbf{I}_s & \mathbf{0} \\ \mathbf{0} & \mathbf{I}_r \end{bmatrix} - \begin{bmatrix} (\mathbf{A}^+ \mathbf{A})_s \\ (\mathbf{A}^+ \mathbf{A})_r \end{bmatrix} \right) \mathbf{w}, \quad (10)$$

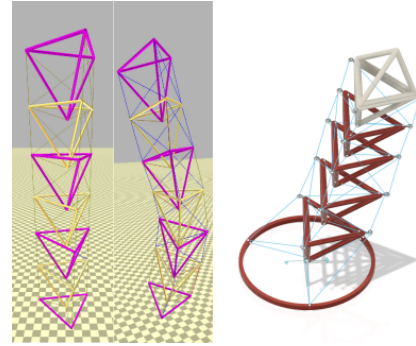


Fig. 5: Left: Upright unactuated HEDRA in equilibrium. Middle: Lateral Bending in HEDRA with actuation in NTRT simulator. Right: CAD rendering of 5-link tensegrity manipulator where the blue lines are cable elements and the elements in red color are bars with end-effector bars in white color

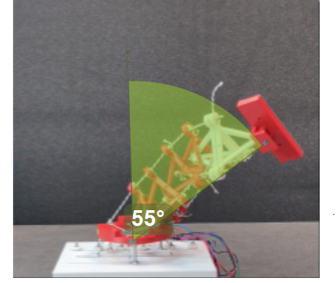
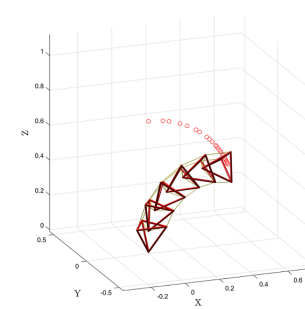


Fig. 6: Simulated trajectory profile of end-effector: Bending configurations. The motion of end-effector was tracked for validating a simulated trajectory and the bending angle was measured, which is shown in the green shaded area and the tracked motion is represented by the arc of the shaded area

An optimal set of cable forces can be found using quadratic programming approach that can be solved in bounded time and can be used for real time control. The optimization problem with an aim to minimize the amount of potential energy in the cables with the unilateral constraint of cables can then be implemented. After obtaining the solution for \mathbf{q} , the rest lengths can be calculated (for example, in the linear elastic case $f_i = K_i(l_i - l_{0i})$):

$$l_{0i} = l_i \left(1 - \frac{q_i}{K_i} \right) \quad (11)$$

B. NTRT Simulation

The NASA Tensegrity Robotics Toolkit (NTRT) [20] is an open-source library for modeling and simulation of tensegrity robots based on the Bullet Physics engine. We have also utilized the features of NTRT simulator that has a custom linear cable model using Hooke's law forces and built the HEDRA robot. The aim of the simulation was to check the rest lengths determined by the inverse kinematic algorithm positioning of the robot in a desired configuration in space as shown in Fig. 5. This was further validated using simulations performed in MATLAB interface as shown in Fig. 6, 7 and 8.

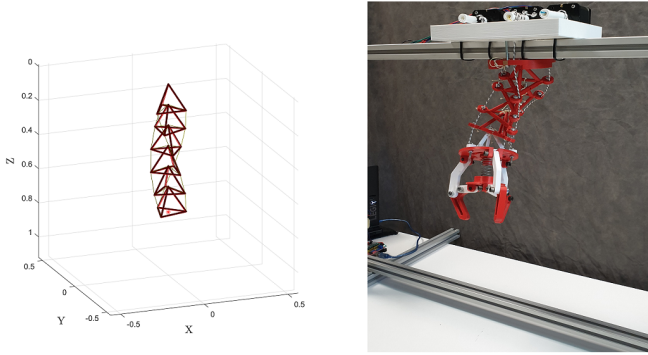


Fig. 7: Simulation (left) and actual prototype (right) in the axial twist configuration.

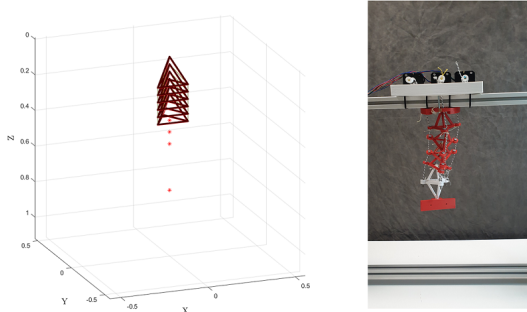


Fig. 8: Simulation (left) and actual prototype (right) in the compression working mode.

V. RESULTS

The simulated trajectory profile of the end-effector is shown in Fig. 9 and the reachable workspace of the robot with the feasible paths within the workspace are shown in Fig. 10. The sequential figures of bending motion generated by different tensile forces and the compact configurations of the HEDRA robot is shown in Fig. 11. Experiments were conducted in three phases. Firstly, the working phases based on different type of actuation scheme of cables were investigated. Secondly, characterization of load capacity of the HEDRA robot with the bending stiffness evaluation was performed. Thirdly, the range of motion was evaluated for bending modes using a motion analysis software.

The performance of the integrated tensegrity robot was evaluated by employing the three types of actuation modes. The bending of the robot driven by tensile force exerted by only one cable, two cable and all three cables in tension for the minimally actuated prototype. The prototype was mounted on to the base and a simple position control was performed using Arduino IDE. The serial-parallel compliant structure facilitated the possibility of simple control. By providing one tensile force to the distal end of the robot, lateral bending was observed (normal to the path of cable in tension) and the maximum bent angle was observed to be larger than 120 degrees and the change in cable length was noted. The manipulator exhibits characteristics of variable stiffness by choosing the number of cables being pulled/

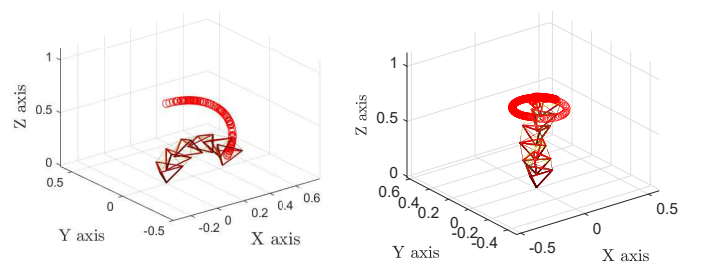


Fig. 9: Simulated motion range for bending and axial twist configurations in $[-\pi/12 \pi/12]$

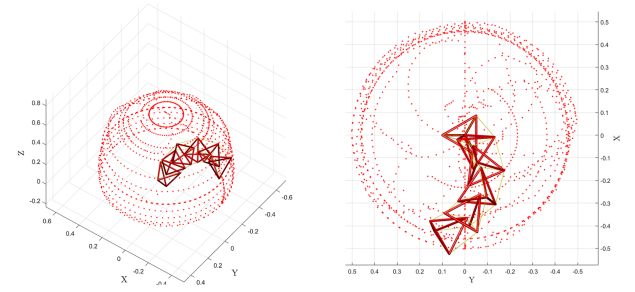


Fig. 10: Reachable workspace (left) and the top view of the feasible motion paths within the workspace (right) of HEDRA

actuated. By pulling two opposite cables, directional stiffness can be achieved and bending happens normal to the path of cable not in tension. The maximum bent angle is lesser than the one observed in the first actuation mode. When all three cables are pulled at the same time, pure contraction happens and manipulator becomes fully stiff. To characterize the load capacity, the thread of the tensegrity structure was pulled by a weight through a pulley that were mounted on the fixture. The distal end of the robot was pulled by adding a set of weights (indicated by the value in the load cell) to generate a deflection. The experimental platform is shown in Figure. 12. The loads were applied along the orthogonal planes (i.e. planes x-z and y-z with z as the vertical direction) which caused displacements in the x and y directions. For this study, the maximum displacement was $x=y= 100$ mm. We can observe from the Fig. 12, a linear load-displacement characteristics is seen till 50 mm for the evaluation in the x-z plane.

The assessment of the bending angle, range of motion of the end-effector was performed using Kinovea, a tool used for motion analysis and tracking [21]. Each motion of the manipulator was tracked for validating a simulated trajectory and the bending angle was measured. The range of motion for the manipulator bending from the vertical position shown in Fig. 6 at an intermediate position. The ROM was evaluated considering the vertical position of the manipulator as reference configuration and is from -77 degrees to +77 degrees with a standard deviation of 2.5 degrees with one tensile force, while with two tensile forces the robot exhibited both bending and axial twist spanning the workspace as shown in Fig. 10.

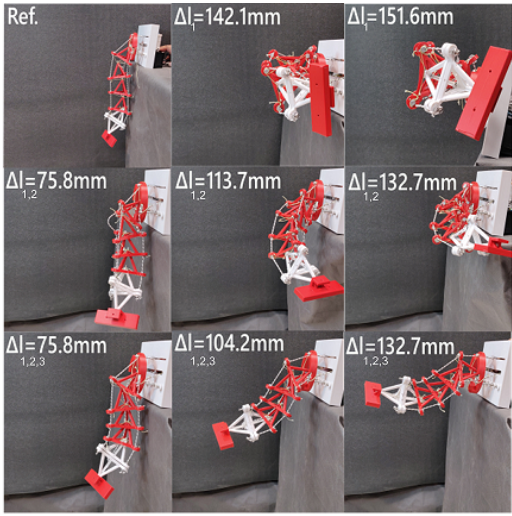


Fig. 11: Sequential figures of bending generated by single force (Top), two tensile forces (Middle) and three forces (Bottom) shows the working phases of HEDRA. The first configuration is the reference configuration

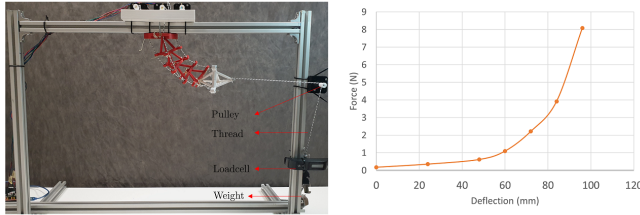


Fig. 12: Left: Experimental platform to evaluate the stiffness variation of the tensegrity manipulator, Right: Force-deflection characteristic curve of tensegrity robot with varied weight to pull the thread with the robot at bent position in the x-z plane(force F_x , displacement x)

A video containing the experimental validation of the proposed robot can be found at the following URL: <https://www.youtube.com/user/PMARrobotics>

VI. CONCLUSIONS

This article provides a novel reconfigurable modular robot by integrating tensegrity-enabled compliant modules. The design process of the bio-tensegrity manipulator in three-dimensions based on the tetrahedral parallel structure linked by tensegrity joint is presented. The tensegrity joint augmented the omnidirectional compliance to the manipulator which can be safer to operate alongside humans. The horizontal saddle cables provides a high translational stiffness and supports the tensegrity joint in suspension while the active cables maintain the antagonistic rotational stiffness in the bending direction. A prototype of the novel robot with six integrated modules was fabricated and the proof-of-concept was demonstrated showing the bending, axial twist and contraction.

REFERENCES

- [1] M. Post and J. Li, "Proof of concept study for small planetary rovers using tensegrity structure on venus," in *16th Reinventing Space Conference*, 2018.
- [2] J. Rieffel and J.-B. Mouret, "Adaptive and resilient soft tensegrity robots," 2018.
- [3] C. H. Belke and J. Paik, "Mori: a modular origami robot," *IEEE/ASME Transactions on Mechatronics*, vol. 22, no. 5, pp. 2153–2164, 2017.
- [4] J. M. Friesen, J. L. Dean, T. Bewley, and V. SunSpiral, "A tensegrity-inspired compliant 3-dof compliant joint," in *2018 IEEE International Conference on Robotics and Automation (ICRA)*. IEEE, 2018, pp. 1–9.
- [5] B. R. Tietz, R. W. Carnahan, R. J. Bachmann, R. D. Quinn, and V. SunSpiral, "Tetraspine: Robust terrain handling on a tensegrity robot using central pattern generators," in *2013 IEEE/ASME International Conference on Advanced Intelligent Mechatronics*. IEEE, 2013, pp. 261–267.
- [6] B. Chen and H. Jiang, "Swimming performance of a tensegrity robotic fish," *Soft robotics*, vol. 6, no. 4, pp. 520–531, 2019.
- [7] J. Shintake, D. Zappetti, T. Peter, Y. Ikemoto, and D. Floreano, "Bio-inspired tensegrity fish robot," in *2020 IEEE International Conference on Robotics and Automation (ICRA)*. IEEE, 2020, pp. 2887–2892.
- [8] J. Friesen, A. Pogue, T. Bewley, M. de Oliveira, R. Skelton, and V. SunSpiral, "Ductt: A tensegrity robot for exploring duct systems," in *2014 IEEE International Conference on Robotics and Automation (ICRA)*. IEEE, 2014, pp. 4222–4228.
- [9] J. Zha, X. Wu, J. Kroeger, N. Perez, and M. W. Mueller, "A collision-resilient aerial vehicle with icosahedron tensegrity structure," *arXiv preprint arXiv:2003.03417*, 2020.
- [10] G. Scarr, *Biotensegrity*. Handspring Publishing, United Kingdom, 2014.
- [11] T. Flemons, "The bones of tensegrity," See http://www.intensiondesigns.com/bones_of_tensegrity, 2012.
- [12] S. Lessard, J. Bruce, E. Jung, M. Teodorescu, V. SunSpiral, and A. Agogino, "A lightweight, multi-axis compliant tensegrity joint," in *2016 IEEE International Conference on Robotics and Automation (ICRA)*. IEEE, 2016, pp. 630–635.
- [13] S. Lessard, D. Castro, W. Asper, S. D. Chopra, L. B. Baltaxe-Admony, M. Teodorescu, V. SunSpiral, and A. Agogino, "A bio-inspired tensegrity manipulator with multi-dof, structurally compliant joints," in *2016 IEEE/RSJ International Conference on Intelligent Robots and Systems (IROS)*. IEEE, 2016, pp. 5515–5520.
- [14] S. M. Levin, "Putting the shoulder to the wheel: a new biomechanical model for the shoulder girdle," *Biomedical sciences instrumentation*, vol. 33, pp. 412–417, 1997.
- [15] A. P. Sabelhaus, H. Ji, P. Hylton, Y. Madaan, C. Yang, A. M. Agogino, J. Friesen, and V. SunSpiral, "Mechanism design and simulation of the ultra spine: a tensegrity robot," in *International Design Engineering Technical Conferences and Computers and Information in Engineering Conference*, vol. 57120. American Society of Mechanical Engineers, 2015, p. V05AT08A059.
- [16] J. C. Case, J. Gibert, J. Booth, V. SunSpiral, and R. Kramer-Bottiglio, "Spinal helical actuation patterns for locomotion in soft robots," *IEEE Robotics and Automation Letters*, vol. 5, no. 3, pp. 3814–3821, 2020.
- [17] T. G. Thuruthel, E. Falotico, M. Manti, and C. Laschi, "Stable open loop control of soft robotic manipulators," *IEEE Robotics and Automation Letters*, vol. 3, no. 2, pp. 1292–1298, 2018.
- [18] F. Visentini, A. K. Mishra, G. A. Naselli, and B. Mazzolai, "Simplified sensing and control of a plant-inspired cable driven manipulator," in *2019 2nd IEEE International Conference on Soft Robotics (RoboSoft)*. IEEE, 2019, pp. 422–427.
- [19] H.-J. Schek, "The force density method for form finding and computation of general networks," *Computer methods in applied mechanics and engineering*, vol. 3, no. 1, pp. 115–134, 1974.
- [20] "NASA tensegrity robotics toolkit (ntrt)." [Online]. Available: <http://ti.arc.nasa.gov/tech/asr/intelligent-robotics/tensegrity/ntrt/>
- [21] N. M. N. Adnan, M. N. A. Ab Patar, H. Lee, S.-I. Yamamoto, L. Jong-Young, and J. Mahmud, "Biomechanical analysis using kinovea for sports application," in *IOP conference series: materials science and engineering*, vol. 342, no. 1. IOP Publishing, 2018, p. 012097.